Supplement of Atmos. Meas. Tech., 15, 5207–5217, 2022
https://doi.org/10.5194/amt-15-5207-2022-supplement

Atmospheric Measurement Techniques
Open Access
EGU

Supplement of

Thermal–optical analysis of quartz fiber filters loaded with snow samples – determination of iron based on interferences caused by mineral dust

Daniela Kau et al.

Correspondence to: Daniela Kau (daniela.kau@tuwien.ac.at)

Table S1: Temperature set points and residence times of the EUSAAR2 protocol used for thermal-optical analysis with the Lab OC-EC Aerosol Analyzer (Sunset Laboratory Inc.).

Step	Temperature (°C)	Duration (s)
He 1	200	120
He 2	300	150
He 3	450	180
He 4	650	180
He 5*	1	30
He/O_2 1	500	120
He/O_2 2	550	120
He/O_2 3	700	70
He/O_2 4	850	80
CalibrationOx	1	110

*EUSAAR2 includes a cooling step (He 5) before switching to an oxidizing atmosphere

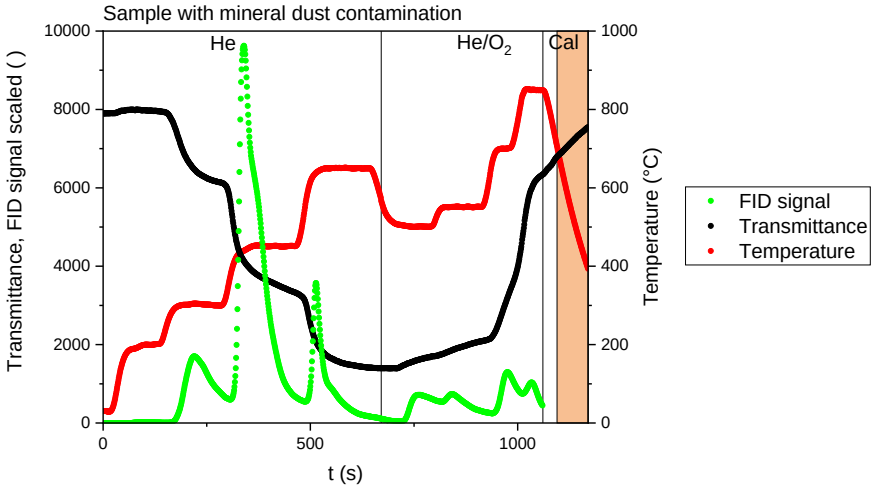

Figure S1: Thermogram of a sample containing MD.

The FID signal (green) shows higher amounts of OC in the sample than EC. The high FID signal caused by the calibration gas at the end of the measurement is not shown. An automatic split point could not be set for the sample, as the transmittance (scaled to be between 1390 and 8000 a.u.) does not reach its initial value during the measurement (black line). Using the transmittance at 250°C as a reference value for the split point would not yield EC concentrations, while a split point could be set using the transmittance at 550°C.

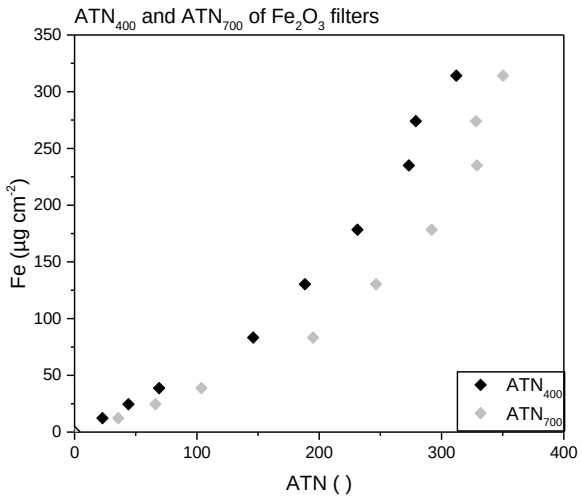

Figure S2: Relationship of Fe loading and ATN_{700} and ATN_{400} of filters loaded with reference material (Fe_2O_3).

As the transmittance values of the unloaded quartz fiber filters at room temperature could not be determined retrospectively, the median transmittance of 14 unloaded blank filters (3352 a.u.) was used to approximate I_0. ATN_{400} and ATN_{700} relate the transmittance at the respective temperatures to this median value. The data pairs (ATN_{400} and ATN_{700}) determined for each Fe loading refer to the same filter and compare well, although the value of I_0 is approximated. Obvious differences in the true values of I_0 lead to the inconsistencies observed between the data pairs, which are more pronounced at the upper end of the curves. At low Fe loadings the relationship between ATN_{400} and ATN_{700} can be approximated by a linear relationship, but saturation due to artefacts related to filter effects is observed at higher loadings. This effect occurs earlier for ATN_{700}.

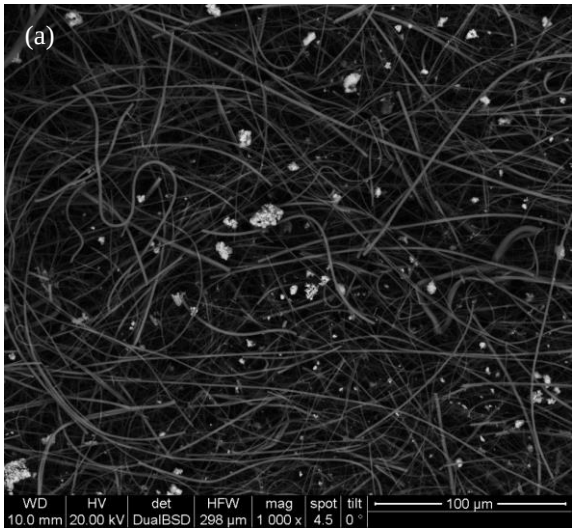
(a)
WD
10.0 mm
HV
20.00 kV
det
DualBSD
HFW
298 µm
mag
1 000 x
spot
4.5
tilt
0 °
100 µm

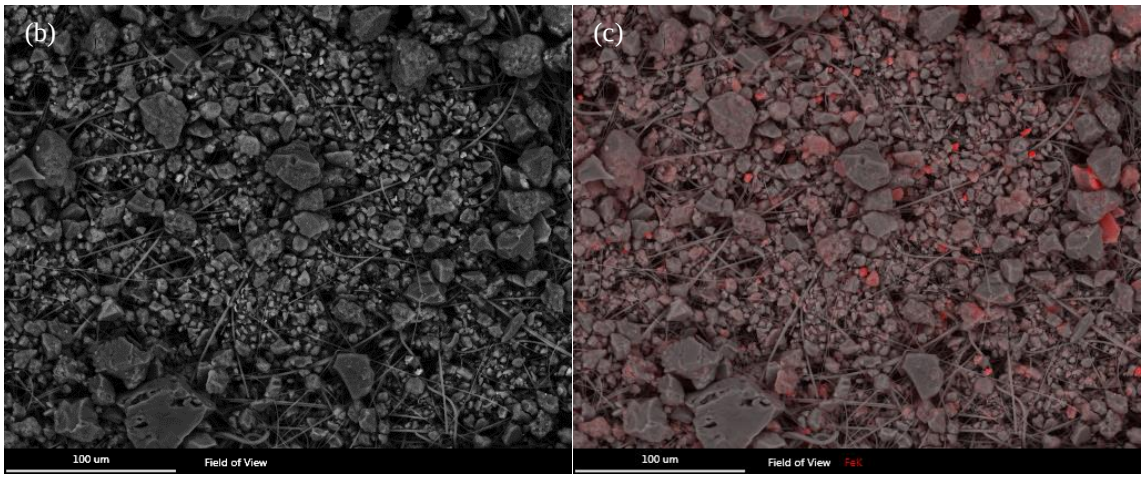
(b)
100 um
Field of View
(c)
100 um
Field of View
FeK

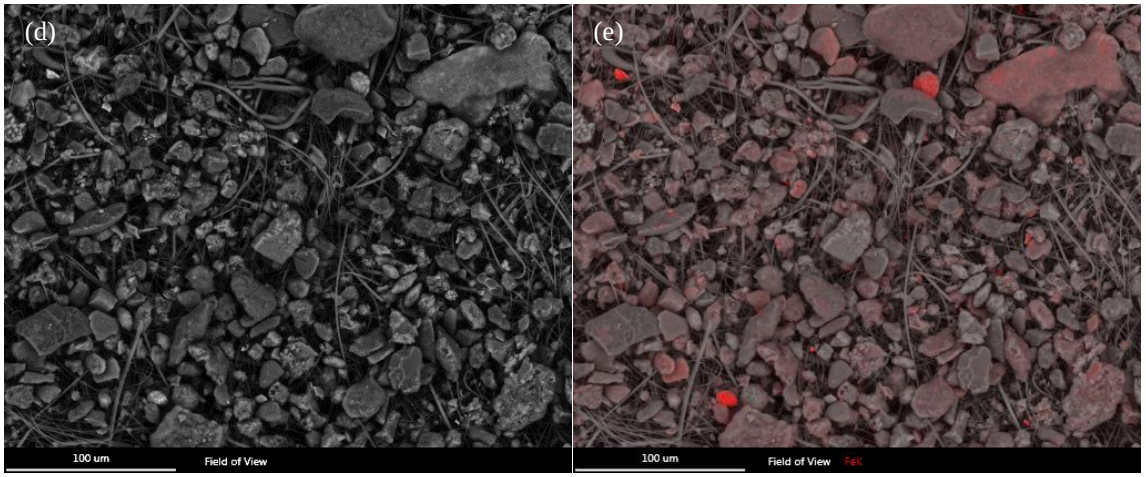
(d)
100 um
Field of View
(e)
100 um
Field of View
FeK

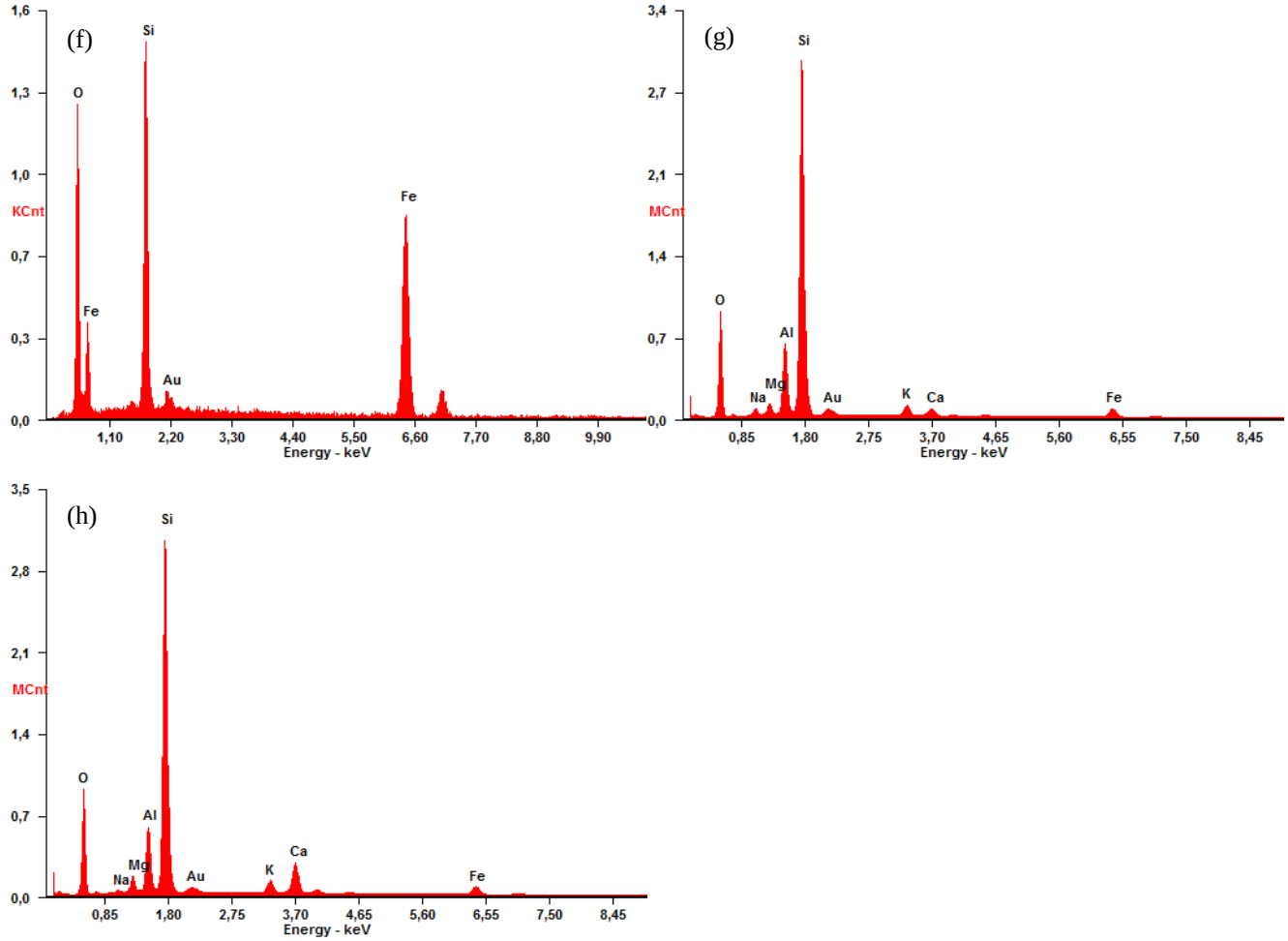

Figure S3: SEM images of a quartz fiber filter loaded with reference material Fe_2O_3 (a), with SRM 2709 (b) and with particles of a liquid snow sample (d). Elemental maps of Fe of these quartz fiber filters loaded with SRM 2709 (c) and with particles of a liquid snow sample (e). EDS spectra of the filters loaded with reference material Fe_2O_3 (f), with SRM 2709 (g) and with particles of a liquid snow sample (h).

The images (a), (b) and (d), recorded using backscattered electrons, show the atomic number contrast. Due to Fe's high atomic number, particles containing Fe are shown in a brighter color than the filter material or particles with different composition. Furthermore, they present an indication of particle sizes and number concentrations. The elemental maps of the filters loaded with SRM 2709 (c) and with particles of a liquid snow sample (e) show areas with high Fe concentrations colored in red. The EDS spectrum for the filter loaded with Fe_2O_3 (f) shows only signals of Si, O, Fe and Au. Besides Fe_2O_3, the filter material, SiO_2, is visible in the spectrum as well as the coating of the sample, Au. The EDS spectra of the filter loaded with SRM 2709 (g) and particles of a liquid snow sample (h) show signals of Ca, K, Si, Al, MG, Na, O, Fe and Au and thus underline the occurrence of different minerals.

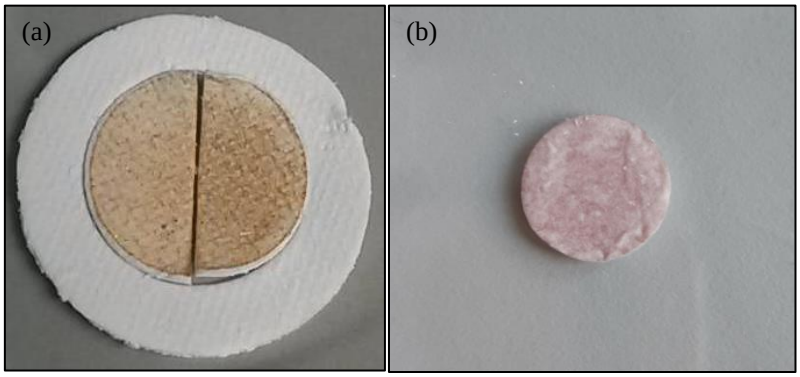

Figure S4: Photos of a filter loaded with liquid snow containing MD (a) and a filter sampled in the railway tunnel (b) after TOA.

Different coloring of residues remaining on the quartz fiber filters loaded with liquid snow and collected in the railway tunnel after TOA becomes visible after TOA and points to different Fe compounds.

Table S2: $ATN_{700-400}$ and Fe concentrations of samples.

Sample	$ATN_{700-400}$ ( )	Fe (µg cm^{-2})	Sample	$ATN_{700-400}$ ( )	Fe (µg cm^{-2})
Snow samples			SRM 2709		
Snow1	22.6	80.3	SRM1	2.7	2.9
Snow2	22.6	52.1	SRM2	39.7	103
Snow3	29.3	115	SRM3	46.3	182
Snow4	17.4	48.4	SRM4	36.3	88.7
Snow5	33.9	200	SRM5	41.7	118
Snow6	28.9	237	SRM6	27.1	48.6
Snow7	26.0	83.5	SRM7	12.2	15.5
Snow8	34.4	136	SRM8	3.1	5.9
Snow9	23.3	270	SRM9	33.4	61.4
Snow10	26.6	75.7	SRM10	47.2	141
Snow11	5.0	18.7	Railway tunnel PM_{10}		
Snow12	30.4	104	RT1	5.7	153
Snow13	33.1	169	RT2	2.7	26.1
Snow14	25.4	69.5	RT3	4.6	172
Snow15	11.1	30.9	RT4	5.3	191
Snow16	14.8	43.9	RT5	5.5	241
Snow17	11.8	27.6	RT6	5.0	199
Snow18	27.4	80.9	RT7	6.3	128
Snow19	30.4	122	RT8	4.8	287
Snow20	36.2	162	RT9	7.6	229
Snow21	35.2	202	RT10	2.4	82.8
Snow22	-2.2	0.4	RT11	4.5	96.0
Snow23	28.4	77.0	RT12	5.0	93.1
Snow24	37.1	127	RT13	8.9	189
Snow25	35.7	171	RT14	6.1	119
Snow26	-1.7	0.7	RT15	3.7	135

Snow27	0.1	5.1	RT16	5.0	63.4
Snow28	6.6	14.9	RT17	4.6	73.8
Snow29	14.9	47.1	RT18	6.0	93.8
Snow30	17.9	50.3	RT19	8.4	121
Snow31	25.7	67.1	RT20	2.6	62.2
Snow32	13.9	28.8	RT21	5.5	158
Snow33	-0.3	3.3	RT22	5.0	171
Snow34	0.5	4.4	RT23	4.6	101
Snow35	3.9	9.8	RT24	2.1	42.4
Snow36	4.4	11.7	RT25	3.0	49.7
Snow37	10.3	24.3	RT26	5.9	103
Snow38	9.8	26.5	RT27	0.3	325
Snow39	15.6	39.0	RT28	1.1	258
Snow40	13.3	39.4	RT29	2.4	36.1
Snow41	22.9	48.0	RT30	2.2	263
Snow42	18.1	52.0	RT31	1.3	105
Snow43	19.9	59.2	RT32	2.0	85.1
Snow44	21.1	62.0	RT33	-3.3	30.2
Snow45	-1.6	1.5	RT34	-0.3	133
Snow46	28.0	85.1	RT35	7.1	201
Snow47	15.2	44.8	RT36	2.1	295
Snow48	33.4	191	RT37	0.2	183
Snow49	23.8	72.6	RT38	2.8	237
Snow50	29.6	142	RT39	3.4	137
Snow51	-2.1	1.3	RT40	-1.7	53.5
Snow52	30.0	220	RT41	2.4	79.4
Snow53	21.9	289	RT42	1.4	39.2
Snow54	7.0	27.7	RT43	-0.6	24.9
Snow55	11.5	29.7	RT44	-2.3	35.2
Snow56	20.0	56.7	RT45	-0.3	63.8
Snow57	31.7	160	RT46	1.3	55.8
Snow58	22.6	109	RT47	1.1	48.0
Snow59	28.5	317	RT48	-0.9	42.6
High alpine PM_{10}			RT49	-1.8	25.4
SBK1	0.1	8.3	RT50	-2.1	57.2
SBK2	0.8	6.0	RT51	0.3	163
SBK3	0.5	3.5	RT52	2.0	92.6
SBK4	0.6	6.4	RT53	1.6	16.4
SBK5	-0.7	4.2	RT54	0.9	111
SBK6	-2.5	1.1	RT55	1.7	191
SBK7	-1.2	4.6	RT56	3.9	164

SBK8	-0.4	10.3	RT57	3.5	179
SBK9	8.1	15.9	RT58	-1.6	17.2
SBK10	6.5	14.9	RT59	-0.2	45.3
SBK11	6.4	21.1	RT60	-0.7	76.0
SBK12	6.3	19.1	RT61	-0.8	69.1
SBK13	8.6	32.2	RT62	1.2	191
SBK14	14.1	30.7	RT63	0.5	151
Reference Fe_2O_3			RT64	1.2	99.8
Fe1	-1.6	0.5	RT65	0.0	130
Fe2	12.9	12.3	RT66	-2.6	13.7
Fe3	22.1	24.6	RT67	2.6	77.1
Fe4	34.6	38.7	RT68	6.3	171
Fe5	49.0	83.2	RT69	1.5	167
Fe6	58.2	130	RT70	-0.8	62.3
Fe7	60.7	178	RT71	0.5	18.0
Fe8	55.6	235	RT72	3.7	88.3
Fe9	49.2	274	RT73	1.0	177
Fe10	38.2	314	RT74	2.2	164
Fe11	9.7	8.8	RT75	1.7	173
Fe12	17.8	19.0	RT76	1.1	91.0
			RT77	-0.8	81.0
			RT78	-2.1	37.8
			RT79	-3.9	7.8